Eur. Phys. J. D **22**, 131–140 (2003)
DOI: 10.1140/epjd/e2002-00217-9

THE EUROPEAN PHYSICAL JOURNAL D

Optical phase-space reconstruction of mirror motion at the attometer level

T. Briant, P.F. Cohadon, M. Pinard, and A. Heidmann[a]

Laboratoire Kastler Brossel[b], Case 74, 4 place Jussieu, 75252 Paris Cedex 05, France

Received 9 July 2002
Published online 29 October 2002 –

Abstract. We describe an experiment in which the quadratures of the position of an harmonically-bound mirror are observed at the attometer level. We have studied the Brownian motion of the mirror, both in the free regime and in the cold-damped regime when an external viscous force is applied by radiation pressure. We have also studied the thermal-noise squeezing when the external force is parametrically modulated. We have observed both the 50% theoretical limit of squeezing at low gain and the parametric oscillation of the mirror for a large gain.

PACS. 42.50.Lc Quantum fluctuations, quantum noise, and quantum jumps – 05.40.Jc Brownian motion – 04.80.Nn Gravitational wave detectors and experiments

1 Introduction

Optomechanical coupling, that is the cross-coupling between the motion of a mirror and a laser field reflected upon it, first appeared in the context of interferometric gravitational-wave detection [1,2] with the existence of the so-called Standard Quantum Limit [3–5]. The unique sensitivity of interferometric techniques has since then been used for other high-sensitivity measurements, such as AFM [6] or optical transducers [7,8]. The field has recently encountered much attention and has gained a life of its own in the quantum optics community: several schemes involving a cavity with a movable mirror have been proposed either to create non-classical states of both the radiation field [9,10] and of the motion of the mirror [11–13], or to perform QND measurements [14]. Recent progress in low-noise laser sources and low-loss mirrors have made the field experimentally accessible [15–17].

A recent trend in quantum optics is to fully reconstruct the quantum state of either a mode of the radiation field through the quantum tomography technique [18,19] or a trapped atom [20], but to our knowledge, no such experiment has yet been performed at the quantum level on a mechanical oscillator.

In this paper, we present an experiment which completes the analysis of the motion of a plano-convex mirror given in [15,16,21], reconstructing the phase-space distribution of the motion through the simultaneous classical measurement of both quadratures of the mirror position. The technique is applied to a variety of states of motion: Brownian motion and its cold-damped and squeezed counterparts.

In Section 2 we present the experimental setup used to monitor the motion of the mirror and we describe how the motion in phase-space can be reconstructed. In Section 3 we consider the case of a free mirror at thermal equilibrium and we compare our experimental results to predictions of the fluctuations-dissipation theorem [22]. The experimental setup has also been modified to include an external viscous force applied to the mirror, and a similar analysis is given in Section 4 in the corresponding case of the cold-damped regime. Our results demonstrate that a new equilibrium is obtained with a reduction of thermal noise.

In Section 5 we present an experiment of parametric amplification of the thermal noise [23], below the oscillation threshold. The experimental setup is modified in order to modulate the strength of the viscous force, and squeezing of the thermal noise has been observed. The observation of parametric oscillations of the mirror is finally described in Section 6.

2 Evolution in phase-space

The mirror motion is monitored by an optomechanical displacement sensor. It relies on the sensitivity of the phase of a reflected light beam to mirror displacements. Monitoring such a phase-shift allows to reconstruct the dynamical evolution of the mirror. This phase-shift can be induced by various kinds of mirror motions, either external [17,24] or internal [15,25,26]. The former is important for suspended mirrors since the excitation of pendulum modes

[a] e-mail: heidmann@spectro.jussieu.fr
[b] Unité mixte de recherche du Centre National de la Recherche Scientifique, de l'École Normale Supérieure et de l'Université Pierre et Marie Curie.
Website: www.spectro.jussieu.fr/Mesure

of the suspension system leads to global displacements of the mirror. The latter corresponds to deformations of the mirror surface due to the excitation of internal acoustic modes of the substrate. These various degrees of freedom have however different resonance frequencies and one can select the mechanical response of a particular mode by using a bandpass filter.

In our experiment we detect only frequencies around the fundamental acoustic resonance of the mirror so that the mechanical response is mainly ruled by the behaviour of this particular internal mode. The mirror motion can then be approximated as the one of a single harmonic oscillator characterized by its resonance frequency Ω_M, its quality factor Q, and its mass M. This mass actually corresponds to an effective mass which describes the effective motion of the mirror as seen by the light, that is the deformation of the mirror surface averaged over the beam spot [25–27].

The temporal evolution of the mirror position $x(t)$ is given by linear response theory [28]. Assuming that a force F is applied to the mirror, the displacement $x[\Omega]$ in Fourier space at frequency Ω is related to the force by

$$x[\Omega] = \chi[\Omega] F[\Omega], \tag{1}$$

where $\chi[\Omega]$ is the mechanical susceptibility of the mirror. For a viscously-damped harmonic oscillator it has a Lorentzian behaviour given by

$$\chi[\Omega] = \frac{1}{M(\Omega_M^2 - \Omega^2 - \mathrm{i}\Gamma\Omega)}, \tag{2}$$

where $\Gamma = \Omega_M/Q$ is the damping rate [29].

Depending on the nature of the applied force F, the spectrum of the mirror motion will typically be peaked around the mechanical resonance frequency Ω_M over a frequency span Γ, which is much smaller than Ω_M for a high-Q harmonic oscillator. To study the temporal evolution of the motion in phase-space, it is preferable to describe the motion in the rotating frame in order to remove the intrinsic oscillatory dependence with time. This leads to the two quadratures X_1 and X_2, defined by

$$x(t) = X_1(t)\cos(\Omega_M t) + X_2(t)\sin(\Omega_M t). \tag{3}$$

This equation yields the expression of the two quadratures in Fourier space,

$$X_1[\omega] = x[\Omega_M + \omega] + x[-\Omega_M + \omega], \tag{4}$$
$$X_2[\omega] = -\mathrm{i}(x[\Omega_M + \omega] - x[-\Omega_M + \omega]). \tag{5}$$

Quadratures $X_1(t)$ and $X_2(t)$ vary very slowly with time (over a $1/\Gamma$ timescale), and ω which represents the frequency mismatch $\Omega - \Omega_M$ between the analysis frequency and the mechanical resonance frequency is always considered small as compared to Ω_M.

Expressions of the quadratures in presence of an applied force can be derived from equation (1) by inserting the expressions of $x[\Omega_M + \omega]$ and $x[-\Omega_M + \omega]$ in the definitions of $X_1[\omega]$ and $X_2[\omega]$. We find after simplification,

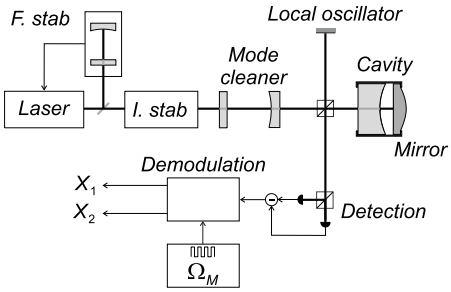

Fig. 1. Experimental setup. A plano-convex mirror is used as the end mirror of a high-finesse cavity. A frequency and intensity-stabilized laser beam is sent into the cavity and the phase of the reflected beam is measured by a homodyne detection. A demodulation system working at the mechanical resonance frequency Ω_M extracts both quadratures of the signal.

$$X_1[\omega] = -\frac{1}{2M\Omega_M}\left(\frac{1}{-\mathrm{i}\omega + \Gamma/2}\right) F_2[\omega], \tag{6}$$

$$X_2[\omega] = \frac{1}{2M\Omega_M}\left(\frac{1}{-\mathrm{i}\omega + \Gamma/2}\right) F_1[\omega], \tag{7}$$

where we have introduced the two quadratures F_1 and F_2 of the applied force, defined in Fourier space by similar expressions as for X_1 and X_2 (Eqs. (4, 5)). Both position quadratures have a Lorentzian response centered at zero frequency and of width Γ.

The harmonic oscillator we consider throughout the paper is the high-Q fundamental acoustic mode of a mirror coated on a plano-convex resonator made of fused silica. The resonator is 1.5 mm thick at the center with a diameter of 14 mm and a curvature radius of the convex side of 100 mm. Such dimensions lead to a resonance frequency of the fundamental mode of the order of 2 MHz. The oscillator's parameters have the following values [15],

$$\Omega_M = 2\pi \times 1\,859 \text{ kHz},\ M = 230 \text{ mg},\ Q = 44\,000. \tag{8}$$

The mirror coated on the flat side of the resonator is used as the end mirror of a single-ended Fabry-Perot cavity with a *Newport high-finesse SuperMirror* as input mirror (Fig. 1). The whole provides a 1 mm-long cavity with an optical finesse $\mathcal{F} = 37\,000$. The light beam entering the cavity is provided by a frequency-stabilized titane-sapphire laser working at $\lambda = 810$ nm. The light beam is also intensity-stabilized and spatially filtered by a mode cleaner.

Near an optical resonance of the cavity the intracavity intensity shows an Airy peak when the cavity length is scanned through the resonance, and the phase of the reflected field is shifted by 2π. The slope of this phase-shift strongly depends on the cavity finesse and for a displacement δx of the end mirror one gets at resonance a phase-shift $\delta\varphi$ on the order of

$$\delta\varphi \simeq 8\mathcal{F}\frac{\delta x}{\lambda} + \delta\varphi_n, \tag{9}$$

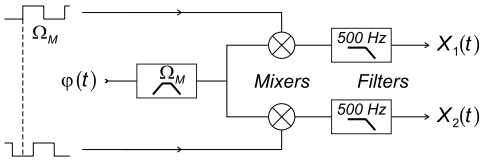

Fig. 2. Demodulation of the position signal: the signal $\varphi(t)$ given by the homodyne detection is filtered and mixed with two $\pi/2$-dephased square signals at the mechanical resonance frequency Ω_M. Low-pass filters are used to extract the low-frequency component of the quadratures.

where λ is the optical wavelength and $\delta\varphi_n$ the phase noise of the reflected beam. At high frequency, all technical noises can be suppressed and the phase noise corresponds to the quantum noise of the incident beam which is inversely proportional to the square root of the light power.

The phase of the reflected field is monitored by a homodyne detection working at the quantum level. For a 100 μW incident laser beam, we have shown that the sensitivity to mirror displacements is limited by the quantum noise of light and it has been measured to

$$\delta x_{\min} = 2.8 \times 10^{-19}\ \mathrm{m}/\sqrt{\mathrm{Hz}}, \tag{10}$$

at an analysis frequency of 2 MHz [15].

To extract both quadratures of the mirror motion we use a demodulation system at frequency Ω_M (Fig. 2). A bandpass filter of width 10 kHz first selects frequencies around the fundamental resonance frequency in the signal given by the homodyne detection. The signal is then mixed with two square signals at frequency Ω_M, one dephased by $\pi/2$ with respect to the other one. Harmonics of the output signals are cancelled out by two electronic low-pass filters. The filters also have to cancel the signal due to other acoustic modes of both the resonator and the coupling mirror. The expected width of the fundamental mode being of the order of 43 Hz and the closest mode 3 kHz above, we use second-order filters with a 500 Hz cut-off frequency. We have checked the transfer function of each filter in order to ensure that the dissymmetry between both channels is less than 1%.

Note that X_1 and X_2 are conjugate quantum observables and therefore cannot be measured simultaneously at the quantum level. This is not in contradiction with our experimental setup since we extract the position quadratures X_1 and X_2 from the phase φ of the reflected field which also contains the quantum phase noise $\delta\varphi_n$ of light (Eq. (9)). A measurement of the quadratures is thus contaminated by the quantum noise of light so that it is not possible to measure simultaneously both quadratures at the quantum level. For this paper this does not constitute a limitation since the signals studied in next sections (thermal noise and external force) are way above the Standard Quantum Limit imposed by the measurement and back-action noises [3–5].

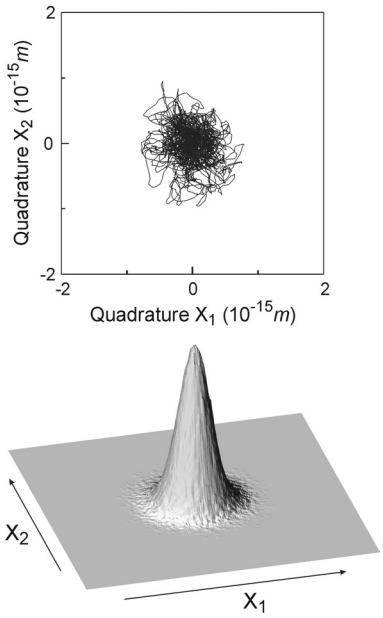

Fig. 3. Brownian motion of the plano-convex mirror in the (X_1, X_2) phase-space. Full scale corresponds to $\pm 2 \times 10^{-15}$ m. Top: temporal acquisition over 500 ms. Bottom: histogram of the distribution acquired over 10 minutes. The number of cells is 256×256, the limit of sensitivity (quantum phase noise of light) corresponding approximately to 1 cell.

3 Observation of Brownian motion

We present in this section the results obtained when the mirror is free (no external force) and at room temperature. The thermal equilibrium can be described as the result of a coupling with a thermal bath *via* a Langevin force F_{T} applied on the mirror. The resulting Brownian motion is the response of the acoustic mode to this force according to equation (1). The fluctuations-dissipation theorem relates the spectrum S_{T} of the Langevin force to the dissipative part of the mechanical susceptibility [22],

$$S_{\mathrm{T}}[\Omega] = -\frac{2k_{\mathrm{B}}T}{\Omega}\mathrm{Im}\left(1/\chi[\Omega]\right), \tag{11}$$

where k_{B} is the Boltzmann constant and T the temperature of the thermal bath.

The sensitivity of our experiment is high enough to detect the Brownian motion. We have already observed the noise spectrum of the mirror displacement, which has a Lorentzian shape centered at the mechanical resonance frequency Ω_M and a width Γ [15]. The height of the peak is at least 4 orders of magnitude larger than the sensitivity defined by the quantum phase noise of the reflected beam (Eq. (10)).

We have observed the temporal evolution of the Brownian motion by sending the outputs of the demodulation system in a digital oscilloscope. The resulting traces of the two quadratures X_1 and X_2 are plotted in the upper curve of Figure 3 for an acquisition time of 500 ms. The temporal trajectory in phase-space appears as a random walk around the center $(X_1 = 0, X_2 = 0)$.

This plot can be compared to the Brownian motion of a mirror coated on a torsion oscillator, as observed in reference [17] by a similar optical interferometry technique. The larger density of points and the more circular shape of our results is due to the larger ratio between the acquisition time $\tau_{\rm acq}$ and the evolution time ($\simeq 2\pi/\Gamma$) of the Brownian motion in phase-space. In our experiment, $\tau_{\rm acq} = 500$ ms and $\Gamma/2\pi = 43$ Hz, so that the phase space is mapped approximately 20 times. In the case of the torsion oscillator, as the mechanical resonance frequency is two orders of magnitude lower, $\Gamma/2\pi \simeq 20$ mHz and the phase space is mapped just once even for a $\tau_{\rm acq} = 80$ s acquisition time. This explains why results in reference [17] look similar to the Brownian motion of a free particle: ergodicity is irrelevant on such short timescales.

Our results are more likely to be compared to the thermomechanical noise observed with an AFM cantilever [23], although the simpler two-wave technique used in this work yielded a lower sensitivity, on the order of 10^{-12} m. In this experiment the resonance frequency also lay in the 20 kHz range but the lower mechanical quality factor of the cantilever drastically lowered the timescale of the Brownian motion, enabling to display results comparable to ours.

We have calibrated the observed displacements by using a frequency modulation of the laser beam. As shown by equation (9) we measure a displacement with a reference corresponding to the optical wavelength. A displacement Δx of the mirror is thus equivalent to a frequency variation $\Delta\nu$ of the laser related to Δx by

$$\frac{\Delta\nu}{\nu} = \frac{\Delta x}{L}, \tag{12}$$

where ν is the optical frequency and L the cavity length. Plots of Figure 3 correspond to a full scale of the oscilloscope of ± 100 mV. We have applied a frequency modulation of calibrated amplitude $\Delta\nu = 200$ Hz and obtained a deviation in phase-space of 27 mV. From equation (12) this corresponds to an equivalent displacement $\Delta x = 5.4 \times 10^{-16}$ m, so that 1 mV is equivalent to 2×10^{-17} m and full scale in Figure 3 corresponds to $\pm 2 \times 10^{-15}$ m.

This calibration also allows to determine the sensitivity of the measurement in phase-space. The quantum phase noise of light induces a rms voltage noise at the output of the demodulation system of 0.86 mV. The smallest observable displacement in phase-space is then

$$\Delta x_{\rm min} = 1.7 \times 10^{-17} \text{ m}, \tag{13}$$

and corresponds to a few attometers. One can relate this sensitivity to the one expressed in term of spectral amplitude (Eq. (10)). Since the phase noise of the reflected beam is a white noise on the frequency scale of the measurement, the minimum measurable displacement $\Delta x_{\rm min}$ in phase-space is equal to the spectral sensitivity $\delta x_{\rm min}$ integrated over the measurement bandwidth, that is

$$\Delta x_{\rm min}^2 = (\delta x_{\rm min})^2 \int |H[\omega]|^2 \, {\rm d}\omega, \tag{14}$$

where $H[\omega]$ is the transfer function of the low-pass filters at the output of the demodulation system. From the value of the spectral sensitivity (Eq. (10)) and the characteristics of the filter (second-order filter with cut-off frequency 460 Hz and quality factor 2 200), one gets

$$\Delta x_{\rm min} \simeq 1.65 \times 10^{-17} \text{ m}, \tag{15}$$

in excellent agreement with the measured value (Eq. (13)). As shown by equation (14) the sensitivity depends on the frequency cut-off of the filters and can be increased with a smaller measurement bandwidth.

Acquiring data during a longer time allows to reconstruct the distribution in phase-space. The full voltage scale at the output of the demodulation system is divided into 256 cells so that one cell approximately corresponds to the limit of sensitivity $\Delta x_{\rm min}$. We then perform an histogram by accumulating the temporal traces of the quadratures in the 256×256 cells. For an acquisition time of 10 minutes the total number of points delivered by the digital oscilloscope is of the order of 6×10^5 and the phase-space is mapped approximately 25 000 times. One then gets a good statistics for the phase-space distribution as shown in the bottom curve of Figure 3. The distribution has a Gaussian shape with a revolution symmetry verified with an agreement better than 1%. The width of the distribution is

$$\Delta X_1 = \Delta X_2 = 36.6 \times 10^{-17} \text{ m}. \tag{16}$$

This result can be compared to the theoretical value expected for the Brownian motion of a harmonic oscillator. The two quadratures $F_{\rm T_1}$ and $F_{\rm T_2}$ of the Langevin force are uncorrelated and have a flat spectrum ($S_{\rm T_1} = S_{\rm T_2} = 2S_{\rm T}$). From equations (6, 7, 11) one gets the spectrum for the two position quadratures

$$S_{X_1}[\omega] = S_{X_2}[\omega] = \frac{\Gamma}{M\Omega_M^2 (\omega^2 + \Gamma^2/4)} k_{\rm B} T. \tag{17}$$

Both noise spectra are centered around zero frequency with a Lorentzian shape of width Γ. Integration over frequency leads to the variances

$$\Delta X_1^2 = \Delta X_2^2 = \frac{k_{\rm B} T}{M\Omega_M^2} \cdot \tag{18}$$

According to the characteristics of the harmonic oscillator (Eq. (8)) one gets dispersions for the two quadratures of 36.3×10^{-17} m in excellent agreement with the experimental value (Eq. (16)).

Finally we have determined the correlation function of the motion in phase-space defined for quadratures X_i, X_j $(i, j = 1, 2)$ as

$$C_{ij}(\tau) = \langle X_i(t) X_j(t+\tau) \rangle_t, \tag{19}$$

where the brackets $\langle ... \rangle_t$ stand for the temporal average over the measurement time. Curves a in Figure 4 show the experimental result obtained for an acquisition time of 10 minutes. As expected for a harmonic oscillator in

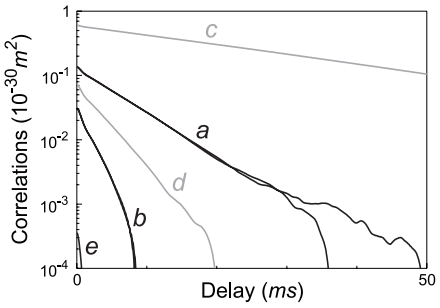

Fig. 4. Plots in lin-log scale of the temporal correlation functions $C_{11}(\tau)$, $C_{22}(\tau)$ for both quadratures as a function of the delay τ; (a) free motion at room temperature; (b) cold damped mirror (Sect. 4); (c and d) parametric cooling (Sect. 5); (e) phase noise of light.

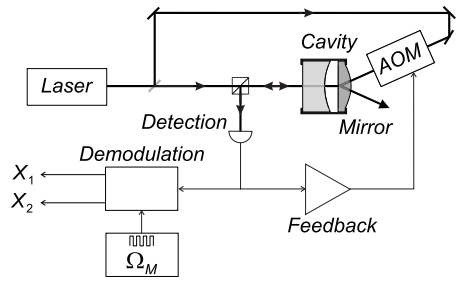

Fig. 5. Cold-damping experimental setup. The mirror is submitted to the radiation pressure of an auxiliary laser beam reflected from the back on the mirror and intensity-modulated by an acousto-optic modulator (AOM). The feedback loop allows to apply an additional viscous force.

thermal equilibrium, there is no cross-correlation between the two quadratures ($C_{12} = C_{21} = 0$) and auto-correlation functions C_{11} and C_{22} are equal and exhibit an exponential decay from their initial values corresponding to the variances,

$$C_{ii}(\tau) = \Delta X_i^2 \exp(-\Gamma\tau/2). \tag{20}$$

The slope of the curve leads to a damping constant $\Gamma/2\pi$ of 48 Hz in good agreement with the expected value ($\Gamma/2\pi \simeq 43$ Hz).

Curve e in Figure 4 represents the correlation function for the phase noise of the reflected beam obtained when the cavity is out of resonance with the incident laser. One gets an exponential decay related to the cut-off frequency of the low-pass filters of the demodulation system. This curve clearly shows that the measurement noise is almost negligible as compared to the thermal noise of the mirror.

4 Cold-damped regime

We now study the temporal evolution of the mirror in the cold-damped regime obtained by freezing the motion with an additional radiation pressure applied on the mirror. The principle of the cold damping mechanism [30] is to monitor the thermal motion and to use an electronic feedback loop which corrects the displacement by applying an appropriate damping force [16].

As shown in Figure 5 an acousto-optic modulator and an intensity-modulated beam is added to the experimental setup. This allows to apply a controlled radiation pressure on the mirror. An electronic differentiator with a variable gain drives the modulator to create a viscous force, that is a force proportional to the measured velocity of the mirror. The incident beam on the modulator is intensity-stabilized in order to apply a well calibrated force.

The effect of this force is to modify the damping of the mirror. It can be described as a change in the mechanical susceptibility which now becomes [16]

$$\chi_{fb} = \frac{1}{M\left(\Omega_M^2 - \Omega^2 + (1+g)\,\Gamma\Omega\right)}, \tag{21}$$

where g is a dimensionless parameter characterizing the gain of the feedback loop and proportional to the electronic gain and to the intensity of the auxiliary beam. As no additional thermal noise is associated with the cooling process, the mirror motion is still described by the evolution equation (1) where the mechanical susceptibility χ is replaced by χ_{fb}. The resulting motion is equivalent to a thermal equilibrium but at a different temperature, depending on the gain g of the loop. The fluctuations-dissipation theorem allows to define an effective temperature $T_{\rm eff}$ which is smaller than the room temperature T for a positive gain g,

$$T_{\rm eff} = \frac{T}{1+g}\cdot \tag{22}$$

The freezing of the mirror of course goes with a reduction of the Brownian motion which would appear as a shrinking of the distribution in phase-space. The variances of quadratures X_1 and X_2 can be calculated in the same way as in previous sections and one gets expressions similar to equation (18) with temperature T replaced by $T_{\rm eff}$,

$$\Delta X_1^2 = \Delta X_2^2 = \frac{k_{\rm B}T}{M\Omega_M^2(1+g)}\cdot \tag{23}$$

The change in the mechanical susceptibility also affects the spectra of X_1 and X_2. They still have a Lorentzian shape but with a width equal to the effective damping $(1+g)\,\Gamma$ and a power at resonance reduced by a factor $(1+g)^2$.

The cold damping of a mirror has already been demonstrated by studying the thermal noise spectrum of the mirror [16,21]. Noise reductions larger than 30 dB at the mechanical resonance frequency and temperature reduction factors larger than 10 have been obtained. We present here the results obtained in phase-space for a moderate gain $g \simeq 3$.

The motion of the cold-damped mirror is shown in Figure 6 (top curve) which also displays the related histogram (bottom curve). As expected this distribution has a Gaussian shape with cylindrical symmetry, but with a reduced width as compared to the initial thermal distribution of Figure 3. Ratios of the variance of the quadratures

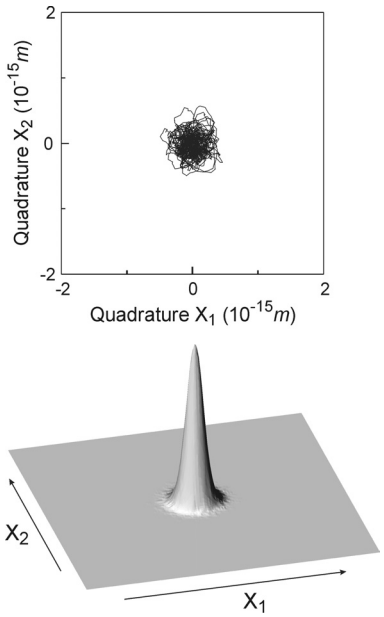

Fig. 6. Cold-damped motion with a gain $g = 3$, in the (X_1, X_2) phase-space (same scale as in Fig. 3). The shrinking of the motion is due to the cooling mechanism. Top: temporal acquisition over 500 ms. Bottom: corresponding histogram acquired over 10 minutes.

between the two situations are in agreement with equation (23) and with the value of the feedback gain.

Curves b in Figure 4 show the auto-correlation functions for the two quadratures. They correspond to the ones of a harmonic oscillator in thermal equilibrium at a lower temperature $T_{\rm eff}$. Compared to the Brownian motion at room temperature, the initial value at $\tau = 0$ is decreased as the variances and the time constant of the exponential decay is reduced. This is associated with the increase of the effective damping by the cold damping mechanism ($(1 + g)\,\Gamma/2\pi \simeq 170$ Hz).

5 Parametric cooling

Distributions obtained in previous sections are symmetric since there is no privileged quadrature. We now explore the possibility to obtain asymmetric distributions, that is to squeeze the thermal noise. By analogy with quantum squeezed states of light, one convenient way to achieve such states is to use parametric amplification. One can take advantage of the presence of an intensity-controlled auxiliary laser beam to modulate some parameters of the mechanical oscillator at twice the resonance frequency Ω_M.

Parametric amplification of a mechanical harmonic oscillator is usually done by modulating its spring constant [23,31]. An equivalent mechanism is obtained for a mirror by applying a modulated force proportional to the position x of the mirror,

$$F(t) = 2gM\Gamma\Omega_M \cos(2\Omega_M t)\, x(t), \tag{24}$$

where g is the gain of the parametric amplification. This can easily be done in our experiment by monitoring the mirror position and accordingly controlling the force applied by the auxiliary beam. Since we use an electronic control it is even possible to differentiate the signal given by the homodyne detection as in the case of cold damping, so that we apply a modulated force proportional to the velocity $\dot{x}$ of the mirror,

$$F(t) = 2gM\Gamma\cos(2\Omega_M t)\,\dot{x}(t). \tag{25}$$

This corresponds to the less usual case of a parametric amplification *via* a modulation of the relaxation rate of the mechanical oscillator.

For such a viscous force one gets from equations (4, 5) the two quadratures F_1 and F_2 of the applied force,

$$F_1[\omega] = gM\Gamma\Omega_M X_2[\omega], \tag{26}$$
$$F_2[\omega] = gM\Gamma\Omega_M X_1[\omega]. \tag{27}$$

According to the evolution equations (6, 7) one finds that the two quadratures X_1 and X_2 of the mirror position are decoupled and obey the following equations,

$$X_1[\omega] = -\frac{1}{2M\Omega_M}\left(\frac{1}{-\mathrm{i}\omega + \Gamma_1/2}\right) F_{\mathrm{T}_2}[\omega], \tag{28}$$
$$X_2[\omega] = \frac{1}{2M\Omega_M}\left(\frac{1}{-\mathrm{i}\omega + \Gamma_2/2}\right) F_{\mathrm{T}_1}[\omega], \tag{29}$$

where F_{T_1} and F_{T_2} are the two quadratures of the Langevin force F_{T} and where Γ_1, Γ_2 are the quadrature-dependent effective dampings in presence of the modulated feedback force,

$$\Gamma_1 = \Gamma(1 + g), \tag{30}$$
$$\Gamma_2 = \Gamma(1 - g). \tag{31}$$

As for the cold damping mechanism, the parametric amplification changes the damping of the oscillator but the effect now depends on the quadrature, one damping being increased while the other one is decreased. As a result, one quadrature of the motion is amplified whereas the other one is attenuated. From equations (28, 29) one gets the variances,

$$\Delta X_1^2 = \frac{k_{\mathrm{B}}T}{M\Omega_M^2}\frac{\Gamma}{\Gamma_1}, \tag{32}$$
$$\Delta X_2^2 = \frac{k_{\mathrm{B}}T}{M\Omega_M^2}\frac{\Gamma}{\Gamma_2}, \tag{33}$$

which have to be compared to equation (18).

In the case of a modulated restoring force (Eq. (24)) the two quadratures F_1 and F_2 of the force respectively depend on X_1 and X_2 so that the evolution equation of X_1 and X_2 are no longer decoupled. One has to consider new quadratures obtained by a rotation of 45° in phase-space in order to obtain decoupled equations similar to equations (28, 29), with the same effective dampings Γ_1 and Γ_2. Both forces thus give the same results except for a global rotation in phase-space.

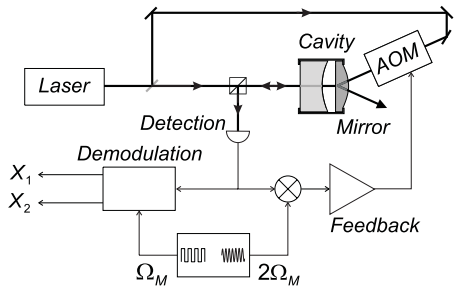

Fig. 7. Experimental setup of parametric amplification. An electronic mixer modulates the signal of the feedback loop at twice the mechanical resonance frequency Ω_M. The demodulation system is synchronized with the reference signal at $2\Omega_M$.

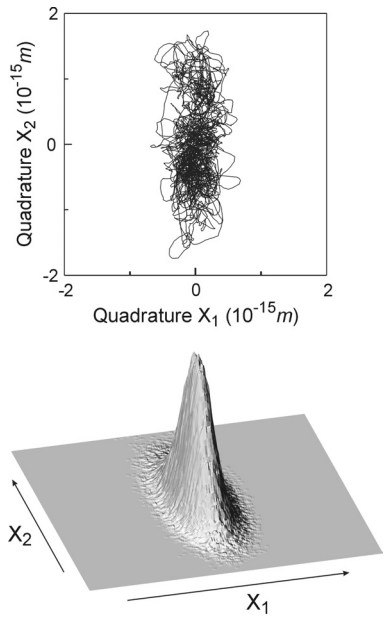

Fig. 8. Parametric amplification of the Brownian motion for a gain $g = 0.8$, in the (X_1, X_2) phase-space (same scale as in Fig. 3). The squeezing of the thermal noise is due to the quadrature-dependent cooling. Top: temporal acquisition over 500 ms. Bottom: corresponding histogram acquired over 10 minutes.

The feedback loop in our experimental setup is modified in order to modulate the amplitude of the force applied by the auxiliary laser beam at twice the resonance frequency Ω_M (Fig. 7). A reference signal is used to synchronize this modulation with the demodulation of the quadratures. We can change the phase between the two signals at Ω_M and $2\Omega_M$ in order to select the decoupled quadratures, either X_1 and X_2 for a modulated viscous force (Eq. (25)) or quadratures rotated by 45° for a modulated restoring force (Eq. (24)).

The resulting motion in phase space is shown in Figure 8 for a parametric gain $g = 0.8$. The distribution still has a Gaussian shape but with different widths for the two quadratures. The distribution is no longer symmetric and dispersions of both quadratures are found equal to

$$\Delta X_1 = 27 \times 10^{-17} \text{ m}, \ \Delta X_2 = 78 \times 10^{-17} \text{ m}. \quad (34)$$

Compared to the dispersion obtained at room temperature (Eq. (16)) the variance of quadrature X_1 is reduced by a factor $1/(1+g)$ whereas the one of quadrature X_2 is increased by a factor $1/(1-g)$. One quadrature is thus cooled while the other one is heated and the state corresponds to a thermal squeezed state.

Curves c and d of Figure 4 show the auto-correlation functions for the two quadratures X_2 and X_1, respectively. Initial values ($\tau = 0$) correspond to the variances deduced from equation (34) and the time constants of the exponential decays are related to the effective dampings Γ_2 for curve c and Γ_1 for curve d, in agreement with equations (30, 31). Note that we have aligned the two quadratures X_1 and X_2 with the axes of the squeezed thermal state by a proper choice of the phase between the two reference signals at Ω_M and $2\Omega_M$. We have then checked that there is no cross-correlation between the two quadratures ($C_{12} = C_{21} = 0$).

The treatment presented here is based on linear response theory and is only valid for a gain g smaller than 1. For a gain equal to 1, the effective damping Γ_2 vanishes (Eq. (31)) and the variance of quadrature X_2 becomes infinite (Eq. (33)). This actually corresponds to the oscillation threshold of the parametric amplification and will be studied in next section.

We have checked the theoretical behaviour of the parametric amplification as a function of the gain g in the linear regime ($g < 1$). We have repeated the experiment for different values of the gain and reported the effective dampings Γ_i and the variances ΔX_i^2 for the two quadratures ($i = 1, 2$). Points in Figure 9 show the experimental results for these parameters, normalized to their respective values in thermal equilibrium at room temperature. The gain g is estimated by an average over the independent values of the effective dampings and the widths of the distributions in phase-space.

The measurements are in very good agreement with the theoretical expressions given by equations (30–33) and shown as solid lines in Figure 9 without any adjustable parameter. Both dampings have linear and opposite dependence with the gain. The variance of quadrature X_2 increases and diverges at the oscillation threshold $g = 1$, whereas the one of quadrature X_1 goes down to 0.5. The efficiency of parametric amplification which is mainly related to the power of the auxiliary laser beam is large enough to obtain a gain g close to unity. One then reaches the 50% theoretical limit of squeezing for the variance of quadrature X_1.

6 Parametric oscillation

As in usual parametric amplification the system oscillates above threshold, that is for a gain g larger than 1. This threshold is actually a consequence of the fact that the gain $g\Gamma$ of parametric amplification becomes equal to the

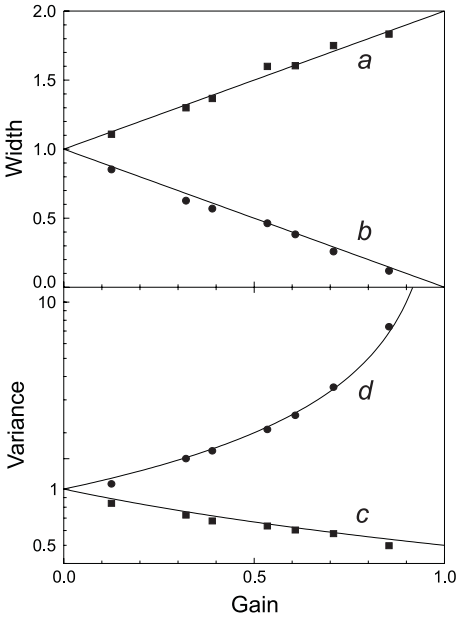

Fig. 9. Relative values of effective dampings Γ_1 (a), Γ_2 (b), and variances ΔX_1^2 (c), ΔX_2^2 (d) normalized to their values in thermal equilibrium at room temperature, for different gains of amplification. Solid lines are theoretical predictions.

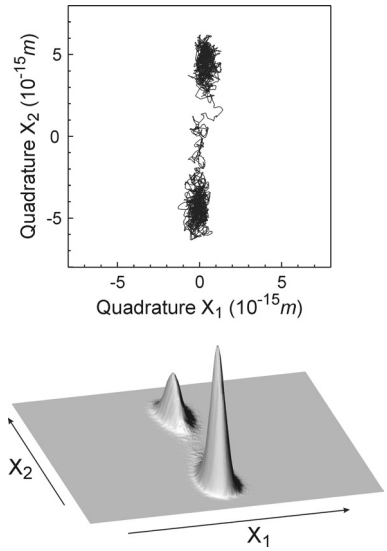

Fig. 10. Parametric oscillation of the mirror for a gain $g > 1$, in the (X_1, X_2) phase-space. Scale is 4 times larger than in Figure 3. Top: temporal acquisition over 500 ms. Bottom: corresponding histogram acquired over 10 minutes. The distribution appears as two opposite squeezed peaks with non-zero equal mean amplitudes.

mechanical losses which are related to the damping Γ. The damping Γ_2 then vanishes and the noise of quadrature X_2 becomes infinite. Above threshold the mirror oscillates at frequency Ω_M in phase with quadrature X_2. The amplitude of oscillation depends both on the gain and on saturation mechanisms which take place in the parametric oscillation regime. In our case they are mainly related to the saturation of the intensity modulation of the auxiliary laser beam.

The distribution of the mirror motion no longer appears as a peak located at the center of phase-space ($X_1 = 0$, $X_2 = 0$). It rather looks like a squeezed distribution centered at a non-zero position along the X_2 axis, the amount of squeezing depending on the distance to threshold. As the modulation of the feedback loop is at frequency $2\Omega_M$, the system is invariant by a π phase-shift and there are two possible positions for the center of the distribution, one for a positive value of $\langle X_2 \rangle$, the other one for a negative and opposite value $-\langle X_2 \rangle$.

Figures 10 and 11 show the experimental temporal evolutions and distributions obtained above threshold, respectively for a gain close to unity and for a larger gain. As expected the distribution in Figure 10 exhibits two peaks along the X_2 axis, symmetrically located with respect to the center. The temporal evolution (top curve in Fig. 10) also shows a concentration of the mirror motion around the two opposite positions. One can however note that the motion sometimes explores the neighbourhood of the center of phase-space and can jump from one position to the other one. Delay between two jumps can be as small as a few seconds for a gain very close to unity and corresponds to a few minutes in the case of Figure 10. Over the 10-minutes acquisition time of the distribution

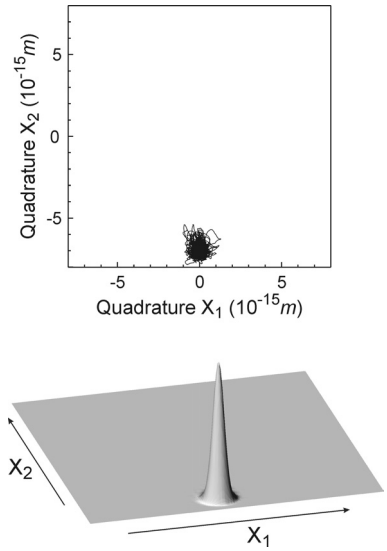

Fig. 11. Parametric oscillation of the mirror for a gain g much larger than 1, in the (X_1, X_2) phase-space (same scale as in Fig. 10). Top: temporal acquisition over 500 ms. Bottom: corresponding histogram acquired over 10 minutes.

the system has actually made only one jump and it has stayed a longer time near the negative position than near the positive one. This explains why the negative peak is higher than the positive one. For a longer acquisition time one would obtain symmetric peaks.

For a larger gain the system can stay a few hours without any jump. During the acquisition time the mirror then stays near one position and the distribution exhibits only one peak as shown in Figure 11.

Parametric oscillation also squeezes the mirror motion along the X_1 quadrature. As usual the squeezing effect is larger close to threshold and the distribution goes back to a disk for large gain (Fig. 11). In contrast with parametric oscillation in optics [32,33], the fluctuations are of the same order as the mean value of the oscillation, that is the distance between the two peaks in Figure 10 is of the same order as their widths. As a consequence one cannot use a linear approach to describe the evolution of fluctuations and the distribution does not appear as an ellipse but as a more complex and distorted shape [34]. It is however possible to evaluate the variance ΔX_1^2 and one obtains in the case of Figure 10 a variance equal to 0.55 times the variance of the thermal noise at room temperature.

Let us finally note that the amplitude of the peaks (distance to the center of phase-space) depends on the gain. One gets a larger amplitude for a higher gain. There is however a limit related to the saturation of the feedback loop. For a very large gain the radiation pressure applied on the mirror is limited by the modulation capabilities of the laser beam intensity. One can easily estimate this limit. When the feedback loop saturates, the intensity modulation tends towards a square signal with a 100% modulation depth. The component of the radiation pressure force at frequency Ω_M is thus on the order of

$$F_{\mathrm{rad}}(t) \simeq 2\frac{P}{c}\frac{4}{\pi}\cos(\Omega_M t), \tag{35}$$

where P is the light power. In this expression $2P/c$ represents the constant force exerted by light without modulation and $4/\pi$ is a correction factor due to the fact that the modulation corresponds to a square signal rather than to a sine one. The response of the mirror is a forced oscillation with a non-zero mean amplitude $\langle X_2 \rangle$ obtained by identifying the intrinsic damping force to the radiation pressure,

$$M\Gamma\Omega_M \langle X_2 \rangle \simeq 2\frac{P}{c}\frac{4}{\pi}\cdot \tag{36}$$

For a 500 mW beam, this corresponds to a mean displacement of 6×10^{-15} m, in very good agreement with the one observed in Figure 11.

7 Conclusion

We have presented an experiment of high-sensitivity displacement measurement, reconstructing the phase-space distribution of a mechanical oscillator with a thousandfold increase in sensitivity upon what had previously been reported. The sensitivity of our experimental setup is currently limited to 1.7×10^{-17} m by the damping timescale of the oscillator, but it could easily be extended to the attometer level by reducing the analysis bandwidth.

Both feedback schemes studied in this paper are able to reduce the thermal noise of the mirror. Their effects however are different. In the case of cold damping the resulting state is still a thermal equilibrium but at a lower effective temperature, in principle down to a zero temperature for a very large gain [35]. One then gets a symmetric Gaussian distribution in phase-space. In contrast, parametric amplification only cools one quadrature of the mirror motion, the other one being heated. One then gets squeezed thermal states with an asymmetric Gaussian distribution in phase-space. This situation is somewhat equivalent to the one which would be obtained with quadrature-dependent feedback loops where the zero-temperature quantum state of the mirror should be reached *via* squeezed thermal states [36].

These results show that the observation of motion in phase-space gives a better understanding and control of optomechanical coupling, on the way to experimental demonstration of related quantum effects.

References

1. C. Bradaschia *et al.*, Nucl. Instrum. Meth. Phys. Res. A **289**, 518 (1990)
2. A. Abramovici *et al.*, Science **256**, 325 (1992)
3. C. Caves, Phys. Rev. D **23**, 1693 (1981)
4. M.T. Jaekel, S. Reynaud, Europhys. Lett. **13**, 301 (1990)
5. V.B. Braginsky, F.Ya. Khalili, *Quantum Measurement* (Cambridge, University Press, 1992)
6. D. Rugar, H.J. Mamin, P. Guethner, Appl. Phys. Lett. **55**, 2588 (1989)
7. M. Stephens, Rev. Sci. Instrum. **64**, 2612 (1993)
8. L. Conti *et al.*, Rev. Sci. Instrum. **69**, 554 (1998)
9. C. Fabre *et al.*, Phys. Rev. A **49**, 1337 (1994)
10. S. Mancini, P. Tombesi, Phys. Rev. A **49**, 4055 (1994)
11. S. Bose, K. Jacobs, P.L. Knight, Phys. Rev. A **56**, 4175 (1997)
12. S. Bose, K. Jacobs, P.L. Knight, Phys. Rev. A **59**, 3204 (1999)
13. S. Mancini, V. Giovannetti, D. Vitali, P. Tombesi, Phys. Rev. Lett. **88**, 120401 (2002)
14. A. Heidmann, Y. Hadjar, M. Pinard, Appl. Phys. B **64**, 173 (1997)
15. Y. Hadjar, P.F. Cohadon, C.G. Aminoff, M. Pinard, A. Heidmann, Europhys. Lett. **47**, 545 (1999)
16. P.F. Cohadon, A. Heidmann, M. Pinard, Phys. Rev. Lett. **83**, 3174 (1999)
17. I. Tittonen *et al.*, Phys. Rev. A **59**, 1038 (1999)
18. K. Vogel, H. Risken, Phys. Rev. A **40**, 2847 (1989)
19. D.T. Smithey, M. Beck, M.G. Raymer, A. Faridani, Phys. Rev. Lett. **70**, 1244 (1993)
20. D. Leibfried *et al.*, Phys. Rev. Lett. **77**, 4281 (1996)
21. M. Pinard, P.F. Cohadon, T. Briant, A. Heidmann, Phys. Rev. A **63**, 013808 (2001)
22. H.B. Callen, T.A. Welton, Phys. Rev. **83**, 34 (1951)
23. D. Rugar, P. Grutter, Phys. Rev. Lett. **67**, 699 (1991)
24. A. Dorsel, J.D. McCullen, P. Meystre, E. Vignes, Phys. Rev. Lett. **51**, 1550 (1983)
25. F. Bondu, J.Y. Vinet, Phys. Lett. A **198**, 74 (1995)
26. A. Gillespie, F. Raab, Phys. Rev. D **52**, 577 (1995)

27. M. Pinard, Y. Hadjar, A. Heidmann, Eur. Phys. J. D **7**, 107 (1999)
28. L. Landau, E. Lifshitz, *Course of Theoretical Physics: Statistical Physics* (Pergamon, New York, 1958), Chap. 12
29. Damping for internal acoustic modes may not be viscous, but as we only consider the motion at frequencies close to the mechanical resonance, there is no observable difference; see P.R. Saulson, Phys. Rev. D **42**, 2437 (1990)
30. J.M.W. Milatz, J.J. van Zolingen, B.B. van Iperen, Physica **19**, 195 (1953)
31. L. Landau, E. Lifshitz, *Course of Theoretical Physics: Mechanics* (Pergamon, New York, 1960), Chap. 5
32. M.J. Collett, C.W. Gardiner, Phys. Rev. A **30**, 1386 (1984)
33. C.W. Gardiner, C.M. Savage, Opt. Commun. **50**, 173 (1984)
34. S. Reynaud, A. Heidmann, E. Giacobino, C. Fabre, in *Progress in Optics XXX*, edited by E. Wolf (North-Holland, Amsterdam, 1992), p. 1
35. J.M. Courty, A. Heidmann, M. Pinard, Eur. Phys. J. D **17**, 399 (2001)
36. D. Vitali, S. Mancini, L. Ribichini, P. Tombesi, Phys. Rev. A **65**, 063803 (2002)